Fermi acceleration in the randomized driven Lorentz gas and the Fermi-Ulam model

A. K. Karlis,* P. K. Papachristou, and F. K. Diakonos†
Department of Physics, University of Athens, GR-15771 Athens, Greece

V. Constantoudis
Institute of Microelectronics, NCSR Demokritos, P.O. Box 60228, Attiki, Greece

P. Schmelcher
Physikalisches Institut, Universität Heidelberg, Philosophenweg 12, 69120 Heidelberg, Germany
and Theoretische Chemie, Im Neuenheimer Feld 229, Universität Heidelberg, 69120 Heidelberg, Germany
(Received 13 March 2007; revised manuscript received 15 June 2007; published 23 July 2007)

Fermi acceleration of an ensemble of noninteracting particles evolving in a stochastic two-moving wall variant of the Fermi-Ulam model (FUM) and the phase randomized harmonically driven periodic Lorentz gas is investigated. As shown in [A. K. Karlis, P. K. Papachristou, F. K. Diakonos, V. Constantoudis, and P. Schmelcher, Phys. Rev. Lett. **97**, 194102 (2006)], the static wall approximation, which ignores scatterer displacement upon collision, leads to a substantial underestimation of the mean energy gain per collision. In this paper, we clarify the mechanism leading to the increased acceleration. Furthermore, the recently introduced *hopping* wall approximation is generalized for application in the randomized driven Lorentz gas. Utilizing the *hopping* approximation the asymptotic probability distribution function of the particle velocity is derived. Moreover, it is shown that, for harmonic driving, scatterer displacement upon collision increases the acceleration in both the driven Lorentz gas and the FUM by the same amount. On the other hand, the investigation of a randomized FUM, comprising one fixed and one moving wall driven by a sawtooth force function, reveals that the presence of a particular asymmetry of the driving function leads to an increase of acceleration that is different from that gained when symmetrical force functions are considered, for all finite number of collisions. This fact helps open up the prospect of designing accelerator devices by combining driving laws with specific symmetries to acquire a desired acceleration behavior for the ensemble of particles.

DOI: 10.1103/PhysRevE.76.016214 PACS number(s): 05.45.Ac, 05.45.Pq

I. INTRODUCTION

In 1949 Fermi [1] proposed an acceleration mechanism of cosmic ray particles interacting with a time dependent magnetic field (for a review, see [2]). Ever since, this has been a subject of intense study in a broad range of systems in various areas of physics, including astrophysics [3–5], plasma physics [6,7], atom optics [8,9], and has even been used for the interpretation of experimental results in atomic physics [10]. Furthermore, when the mechanism is linked to higher dimensional time-dependent billiards, such as a time-dependent variant of the classic Lorentz Gas [11], it has profound implications on statistical, molecular, and solid state physics [12].

Several modifications of the original model have been suggested, one of which is the well-known Fermi-Ulam model (FUM) [13–15] which describes the bouncing of a ball between an oscillating and a fixed wall. FUM and its variants [16,17] have been the subject of extensive theoretical (see Ref. [14] and references therein) and experimental [18–20] studies as they are simple to conceive but hard to understand in that their behavior is quite intricate.

The recurrence equations defining the dynamics of a driven billiard are, in general, of implicit form, which hinders analytical treatment and complicates numerical simulations. For these reasons, a standard simplification, known as the static wall approximation (SWA), originally introduced by Lieberman *et al.* [14], is widely used in the literature. The SWA ignores the displacement of the moving wall but retains the time dependence in the momentum exchange between particle and wall on the instant of collision as if the wall were oscillating. The application of SWA speeds up time-consuming numerical simulations and allows analytical treatment as well as a deeper understanding of the system [14,21–26]. Similar simplified maps have also been used for the investigation of higher-dimensional driven billiards, such as a periodic time-dependent Lorentz gas, consisting of scatterers with time dependent boundaries on a square lattice [12].

However, as has recently been shown by Karlis *et al.* [27] the SWA considerably underestimates particle acceleration. Furthermore, in Ref. [27], through the introduction of the so called *hopping* wall approximation (HWA), which takes into account the spatial motion of the oscillating walls, it was made clear that the failure of the SWA is substantial due to the fact that wall displacement is completely disregarded. More specifically, wall displacement causes small additional fluctuations in the time of free flight between successive collisions, which are ignored by the SWA, leading to the underestimation of the particle acceleration. In the present work, these findings are presented in more detail and an effort is made to clarify the physical mechanism according to which energy exchange between particle and scatterer is affected by

*alkarlis@med.uoa.gr
†fdiakono@phys.uoa.gr

the wall displacement. Moreover, a generalization of the HWA is made to the harmonically driven periodic Lorentz gas, showing that the amount of underestimation in the framework of the *static* approximation is the same as that found in the case of the stochastic harmonically driven FUM. On the other hand, as indicated in Ref. [27], the specific characteristics (symmetries) of the driving law affect the increase with respect to the acceleration. To demonstrate this, additionally to the harmonic driving, sawtooth oscillations are considered, in the context of the original stochastic FUM (with one fixed and one moving wall) as well as for its two-moving wall counterpart. The analysis reveals that the presence of a particular asymmetry in the driving function leads to an increase of acceleration that is different from that acquired when symmetrical force functions are considered, for all finite number of collisions. When the same asymmetric driving is applied on the two-moving wall variant of the FUM, the increase in acceleration due to the displacement of the wall upon collision is once more constant and coincides with that obtained on the assumption of a symmetric force function. The understanding of the effect of the driving law symmetries on the acceleration mechanism, opens up the prospect of combining driving laws with specific symmetries to acquire a desired acceleration behavior for the ensemble of particles.

The paper is organized as follows. In Sec. II the two-moving wall variant of the FUM is presented and all the details needed for the construction of the exact and approximate maps are discussed. In this section we also present the numerical as well as the analytical results in regard with the FUM. The analysis of the Fermi acceleration mechanism for the time-dependent Lorentz gas is presented in Sec. III. In Sec. IV the final remarks are made and conclusions drawn. Finally, some important technical details are discussed in Appendices A and B.

II. FERMI-ULAM MODEL

We explore a dynamical system being a variant of the original FUM. It consists of two harmonically driven infinitely heavy walls with an ensemble of particles bouncing between them. In the following, only the case of noninteracting particles is considered. This FUM variant, with two moving walls instead of one fixed and one moving, is a step towards the understanding of a class of open driven spatially extended billiards. For instance, a FUM with two moving walls fully corresponds to particle motion on a bound orbit that exists between adjacent disks, oscillating in the same direction, in a periodic driven Lorentz gas. When a particle collides with a certain wall, a random shift of the phase of the other wall, which is uniformly distributed in $[0,2\pi)$, occurs. The stochastic component in the oscillation law of the wall simulates the influence of a thermal environment on wall motion and leads to Fermi acceleration [14,21–23,28,29]. It should be noted that although stochasticity can be introduced otherwise—for instance, via a random component in the angular frequency of oscillation—the random phase approach has become quite common as a method of randomization of the FUM and its modifications [12,14,22]. Partially, this is because it is the only conceivable way to randomize the system without changing the energy related quantities, such as the frequency of the moving wall.

The specific setup of the studied system is determined by the oscillation frequencies ω_i and amplitudes A_i of the two walls ($i=L,R$) as well as the distance w between the walls at equilibrium. However, the dynamics does not depend on each of these parameters separately. It is therefore appropriate to introduce the relevant dimensionless quantities $\epsilon_i = A_i/w$ and $r=\omega_L/\omega_R$. Obviously, when the ratio $\chi=\epsilon_L/\epsilon_R$ meets the condition $\chi \gg 1$ (or $\chi \ll 1$) the original FUM is recovered. The case $\chi=1$ ($\epsilon_L=\epsilon_R=\epsilon$) and $r=1$ ($\omega_L=\omega_R=\omega$) is exclusively considered in the following, as the specific choice leads to a considerable reduction of the parameters of the system. Using as a length unit the spacing between the walls w and as a time unit $1/\omega$ the dynamical laws of the system can be written in a dimensionless form:

$$d_{n,(L,R)} = \mp \frac{1}{2} + \epsilon \sin(\delta t_n + t_{n-1} + \eta_n), \tag{1a}$$

$$u_n = \epsilon \cos(\delta t_n + t_{n-1} + \eta_n), \tag{1b}$$

$$V_n = -V_{n-1} + 2u_n, \tag{1c}$$

where $d_{n,(L,R)}$ stands for the position of the (left-right) wall in the instant of the nth collision, u_n stands for the wall velocity, η_n for the random phase component, and V_n for the particle velocity after the nth collision. The time of free flight δt_n is obtained by solving the implicit equation

$$X_{n-1} + V_{n-1}\delta t_n = d_{n,(L,R)}, \tag{2}$$

where X_n stands for the position of the particle in the instant of the nth collision. Equation (2) can be solved numerically, keeping the smallest positive solution. In our computer simulations we implemented the Van Wijngaarden–Dekker–Brent method [30]. Obviously, this equation links the time of the nth collision $t_n=\delta t_n+t_{n-1}$ to the position X_{n-1} of the particle on the $(n-1)$th collision.

A. Static wall approximation

The SWA simplifies the process on the basis of the assumption that the time of free flight, δt_n, depends only on particle velocity, i.e., $\delta t_n = \pm 1/V_{n-1}$. Thus, Eqs. (1) and (2) are simplified to

$$t_n = t_{n-1} \pm \frac{1}{V_{n-1}}, \tag{3a}$$

$$V_n = \pm \left| -V_{n-1} + 2\epsilon \cos(t_n + \eta_n) \right|. \tag{3b}$$

The absolute value in Eq. (3b) is introduced for the following reason: In the high velocity regime, for which the SWA is valid, there is a rare class of collision events in which the direction of the particle velocity is not reversed (within the exact model this corresponds to having multiple collisions with the same wall). In order to prevent the particle from escaping the region between the walls the velocity is re-

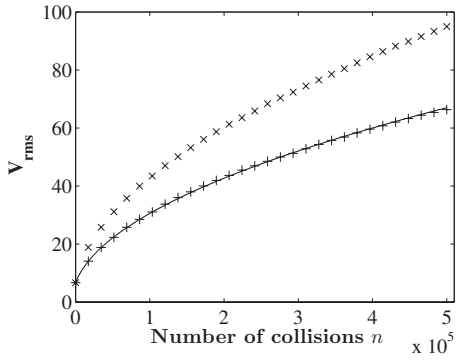

FIG. 1. Numerical results for V_{rms} of an ensemble of 10^4 particles evolving in a stochastic FUM with two oscillating walls as a function of the number of collisions. Results were obtained by iterating the exact ($\times$) as well as the corresponding *static* (+) approximate map, with $\epsilon=1/15$ and $V_0=100/15$. V_{rms} is measured in units of ωw. The analytical result according to the SWA, obtained by averaging over the random phase (solid line), is also shown.

versed "by hand." This is done by taking the absolute value of the particle velocity after such a collision, while the plus (minus) sign corresponds to a collision with the left (right) wall.

If this approximation is applied to the system of two oscillating walls, then it is possible to extract analytically the ensemble averaged change of the square particle velocity $\langle \delta V_n^2 \rangle = \langle V_n^2 - V_{n-1}^2 \rangle$ after integration over the random phase η_n. It should be noted that the ensemble trajectories are characterized by the same initial velocity V_0. From Eq. (1) follows that the square of the modulus of particle velocity is $V_n^2 = V_{n-1}^2 - 4u_n V_{n-1} + 4u_n^2$. Thus

$$\delta V_n^2 = V_n^2 - V_{n-1}^2 = -4u_n V_{n-1} + 4u_n^2. \tag{4}$$

After averaging Eq. (4) over the random phase component we obtain

$$\langle\langle \delta V_n^2 \rangle\rangle = 2\epsilon^2. \tag{5}$$

In Eq. (5) the notation $\langle\langle\ \rangle\rangle$ is used for phase averaging. To extract the ensemble average one should also integrate over the velocity distribution $\rho(|V|,n)$, which in this case is trivial, since the result of Eq. (5) is independent of the particle velocity. Given that $\langle V_n^2 \rangle = \Sigma_{i=1}^n \langle \delta V_i^2 \rangle + V_0^2$, the root mean square particle velocity is

$$V_{\mathrm{rms,SWA}}(n) = \sqrt{2\epsilon^2 n + V_0^2}. \tag{6}$$

Independently, the rms velocity can be obtained numerically, by the iteration of the set of Eqs. (3a) and (3b). Results, yielded by the numerical simulation of an ensemble of 10^4 particles, for $n=5\times10^5$ collisions, with $\epsilon=1/15$ and $V_0=100/15$ are presented in Fig. 1 along with numerical results using the exact Eqs. (1) and (2). Clearly, and despite the external randomization [14] the SWA fails to provide an accurate description of the acceleration process; more specifically, the energy gain of the particles is substantially underestimated. The shortcomings of the SWA must be attributed to the fact that it does not take into account the displacement of the scatterer upon collision. Thus, it is crucial, in order to correctly describe the evolution of the root mean square particle velocity, to incorporate the oscillation of the walls in configuration space.

B. Hopping wall approximation

As mentioned above, one of the advantages of the SWA is the explicit form of Eqs. (3a) and (3b), which facilitates the analytical treatment of the acceleration problem as well as substantially simplifies and speeds up numerical simulations. Therefore, a promising candidate as an alternative to this approximation should also have these merits but at the same time being capable of providing an accurate description of the acceleration process.

For this reason we introduce the so-called *hopping* wall approximation (HWA), which takes into account the effect of the wall displacement. Using this approximation we clarify how the oscillation of the wall in configuration space affects the acceleration law of an ensemble of particles. Furthermore, the corresponding map allows an analytical treatment and is as computationally efficient as the SWA, enabling us to calculate the evolution of the velocity distribution of the particles for long time periods.

The key simplifying assumption of the HWA is that the wall position on the nth collision can be approximated with its position at the previous, $(n-1)$th, collision. This approximation is based on the observation that with increasing particle velocity, the time of free flight decreases, becoming much smaller compared to the oscillation period of the walls and consequently the relative displacement of the wall between two successive collisions becomes very small, i.e., negligible. So, according to the HWA, one wall moves only when a particle collides with the other wall. Thus, when a particle collides with one of the walls, the other "hops" (is instantly moved) to its new position (as defined by the deterministic and random phase component) and remains fixed until the particle collides again with the other wall. However, the velocity of both walls is allowed to oscillate continuously. The equations defining the HWA read

$$d_{n,(L,R)} = \mp \frac{1}{2} + \epsilon \sin(t_{n-1} + \eta_n), \tag{7a}$$

$$u_n = \epsilon \cos(t_n + \eta_n), \tag{7b}$$

$$V_n = \pm |-V_{n-1} + 2u_n|. \tag{7c}$$

As already mentioned in Sec. II A, the absolute value in Eq. (7c) is introduced in order to prevent the particle from traveling beyond the walls. The plus (minus) sign corresponds to a collision with the left (right) wall. The time t_n when the nth collision occurs is determined by Eq. (2), which within the framework of HWA can be solved analytically to obtain

$$t_n = t_{n-1} + \delta t_n^* \pm \frac{1}{V_{n-1}}, \tag{8a}$$

$$\delta t_n^* = \frac{\epsilon[\sin(t_{n-1}+\eta_n)-\sin(t_{n-2}+\eta_{n-1})]}{V_{n-1}}, \tag{8b}$$

where δt_n^* is the correction term to the time of free flight predicted by SWA, due to wall displacement.

In order to obtain the rms particle velocity within the framework of HWA, the mean energy gain per collision $\langle \delta V_n^2 \rangle$ must be calculated. Let us first calculate the average energy gain over the phase of oscillation, $\langle\langle \delta V_n^2 \rangle\rangle$. This is done by averaging Eq. (4) over the random phase component η_n, using the set of Eqs. (8a) and (8b), which leads to the following integrals:

$$I_j = \int_0^{2\pi} \frac{1}{2\pi}[\epsilon \cos(t_n+\eta_n)]^j d\eta_n, \tag{9}$$

where $j=1, 2$ and t_n is given by Eq. (8a). An exact analytical calculation of the integrals I_1, I_2 is not possible. However, for the set of parameters considered here, δt_n^* is much smaller compared to the other phase components. Therefore, we expand the right-hand side (RHS) of Eq. (9) to the leading order of δt_n^*, to obtain

$$I_1 = \frac{1}{2\pi}\int_0^{2\pi} \left[\epsilon \cos\left(\frac{1}{V_{n-1}} + t_{n-1} + \eta_n\right) - \epsilon \sin\left(\frac{1}{V_{n-1}} + t_{n-1} + \eta_n\right)\delta t_n^* \right] d\eta_n, \tag{10}$$

$$I_2 = \frac{1}{2\pi}\int_0^{2\pi} \left[\epsilon^2 \cos^2\left(\frac{1}{V_{n-1}} + t_{n-1} + \eta_n\right) - 2\epsilon^2 \cos\left(\frac{1}{V_{n-1}} + t_{n-1} + \eta_n\right) \times \sin\left(\frac{1}{V_{n-1}} + t_{n-1} + \eta_n\right)\delta t_n^* \right] d\eta_n. \tag{11}$$

After the substitution of Eq. (8b) into Eqs. (10) and (11) the calculation of the integrals yields

$$I_1 \approx -\frac{\epsilon^2 \cos\left(\frac{1}{V_{n-1}}\right)}{2V_{n-1}}, \quad I_2 \approx \frac{\epsilon^2}{2}.$$

Therefore, we find

$$\langle\langle \delta V_n^2 \rangle\rangle \approx 2\epsilon^2 \cos\left(\frac{1}{V_{n-1}}\right) + 2\epsilon^2. \tag{12}$$

At the limit of high particle velocities $V_{n-1} \gg 1$, Eq. (12) is simplified to, $\langle\langle \delta V_n^2 \rangle\rangle \simeq 4\epsilon^2$. Since the result is independent of the particle velocity, the ensemble mean energy gain is

$$\langle \delta V_n^2 \rangle \simeq 4\epsilon^2, \tag{13}$$

which is exactly two times the result obtained by neglecting wall displacement. Consequently, the root mean square velocity as a function of the number of collisions is

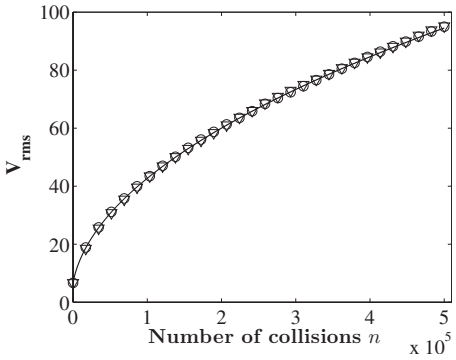

FIG. 2. Numerical results for $V_{\rm rms}$ of an ensemble of 10^4 particles evolving in a stochastic FUM with two oscillating walls as a function of the number of collisions. Results were obtained by iterating the exact (○) as well as the corresponding HWA map (∇), with $\epsilon=1/15$ and $V_0=100/15$. It is noted that $V_{\rm rms}$ is measured in units of ωw. The analytical result according to the HWA, Eq. (14), obtained by averaging over the random phase (solid line), is also shown.

$$V_{\rm rms,HWA}(n) = \sqrt{4\epsilon^2 n + \langle V_0^2 \rangle}. \tag{14}$$

The analytical result of Eq. (14) together with the numerical results obtained by the simulation of 10^4 particles utilizing the HWA map, are shown in Fig. 2. For the sake of comparison, numerical results using the exact map are also presented.

As seen in Fig. 2 the numerical results given by the iteration of the exact and the hopping approximative map virtually coincide. Furthermore, the analytical result of Eq. (14) is also in agreement with the numerical results obtained using the exact map. Obviously, the HWA succeeds in describing particle acceleration, in clear contrast with the SWA which leads to a substantial underestimation. This indicates that the increased particle acceleration is due to the impact of the dynamically induced correlation between the position and velocity of the oscillating wall in the collision process.

C. Physical mechanism

The previous analysis reveals the role of the fluctuations in the time of flight δt_n between successive collisions caused by the displacement of the scatterer. Despite the existence of an external stochastic component in the phase of the oscillating wall these fluctuations lead to a *systematic* increase of the acceleration of the particles. A simple explanation of the physical mechanism leading to the increased acceleration becomes possible by considering the various configurations of the collision processes between the walls and the particles.

Let us assume for a given velocity of the incident particle that the wall is moving in the same direction as the particle after passing the equilibrium position, as shown in Fig. 3. The collision time, as given by the exact map, Eq. (2)—corresponding to the intersection of the particle trajectory with the curve representing the position of the scatterer as a function of time—denoted by t', is increased compared to the time t on the assumption of a wall fixed in space. In Fig. 3 this is shown as the intersection of the particle trajectory

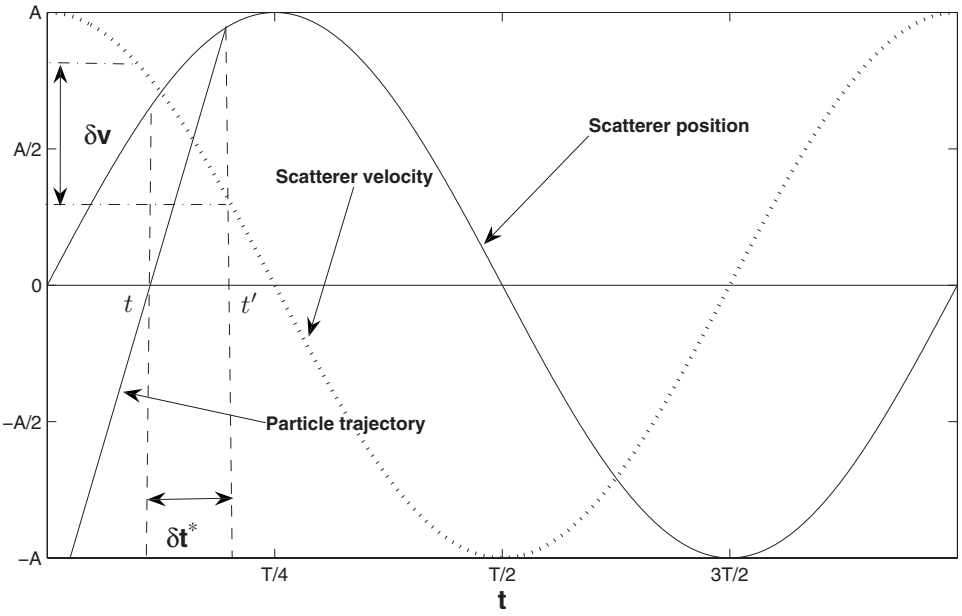

FIG. 3. The position and the velocity of one of the oscillating walls as a function of time. The straight line represents the trajectory of an incident particle.

with the line corresponding to the equilibrium position. In this case, the velocity of the harmonically oscillating wall is a decreasing function of time and therefore an increase of the collision time leads to a decrease of the wall velocity on the actual instant of the collision when compared to the *static wall* approximation. This in turn leads to a reduced energy loss in the course of the collision. This reasoning holds equally for all other types of collisional events, leading to the general picture of reduced energy loss or enhanced energy gain when the wall displacement is taken into account.

It should be stressed that although the additional fluctuations in the time of free flight due to wall displacement lead always to an increased acceleration compared to the acceleration predicted by the SWA, the specific amount of the increase in the energy gain *per collision* due to the wall displacement, depends on the characteristics of the oscillation law. For this reason the ratio $R_h(n)=(\langle V_n^2\rangle - \langle V_0^2\rangle)_{\text{exact}}/(\langle V_n^2\rangle - \langle V_0^2\rangle)_{\text{SWA}}=\Sigma_{i=1}^n\langle \delta V_i^2\rangle_{\text{exact}}/\Sigma_{i=1}^n\langle \delta V_i^2\rangle_{\text{SWA}}$ is introduced, which enables us to compare the relative efficiency of the mechanism leading to the increased acceleration between setups with different driving force laws. The specific definition of $R_h(n)$, compared to that given in Ref. [27], is more convenient for numerical calculations as it converges much more rapidly in terms of ensemble averaging ($\sim 10^5$ initial conditions are adequate for reducing statistical uncertainties to less that 1%, as opposed to numerical simulations using the definition of $R_h(n)$ given in Ref. [27] in which case $>10^6$ initial conditions are necessary). For the harmonically driven FUM (with randomized phase of oscillation) the correction factor $R_h(n)$ can readily be calculated using Eqs. (5) and (12), to obtain

$$R_h(n) = \frac{1}{n}\sum_{i=1}^{n}\left\langle \cos\left(\frac{1}{V_{i-1}}\right)\right\rangle + 1. \tag{15}$$

Due to the Fermi acceleration mechanism developed in the FUM particle velocities quickly acquire large values, i.e., $1/V \ll 1$. The expansion of the right-hand side of Eq. (15) in powers of $1/V$ yields

$$R_h(n) = 2 + O\left(\left\langle \frac{1}{V^2}\right\rangle\right). \tag{16}$$

Consequently, in the case of the two-moving wall variant of the FUM driven by a harmonic driving force and randomized phase of oscillation, the function $R_h(n)$ is (within the leading order of $\langle 1/V\rangle$ approximation) independent of n and equals 2. It should be stressed that this result applies also to the original FUM, with one fixed and one moving wall. Indeed, due to the randomization of the phase of oscillation and the symmetry $u[m(T/2)+T/4-t]=-u[m(T/2)+T/4+t]$ $(m=0,1,2,\ldots)$ of the oscillation time law, the two-wall variant of the FUM becomes fully equivalent to the original FUM, because collisions of the particles with either side of the moving wall(s), on the average, result to the same energy transfer. However, we will show that this is not the case when this particular symmetry of the oscillation law is broken.

D. Sawtooth driving law

In order to demonstrate the variability of the factor R_h and its dependence on the characteristics of the oscillation law, we perform an analysis of the case of a sawtooth driving law, in the context of the original FUM—consisting of one moving and one fixed wall—as well as the two-moving wall FUM variant. In all occasions the phase of the oscillating wall(s) is(are) shifted randomly (according to a uniform distribution) after each collision with a particle. The following class of time-periodic laws for the moving wall(s) are considered:

$$x_i(t) = x_{0,i} + \begin{cases} \frac{1}{a}\frac{(t+\eta)A}{T}, & \frac{(t+\eta)}{T} \in [0,a), \\ -\frac{2}{b-a}\frac{(t+\eta)A}{T}, & \frac{(t+\eta)}{T} \in [a,b], \\ \frac{1}{1-b}\frac{(t+\eta)A}{T}, & \frac{(t+\eta)}{T} \in (b,1], \end{cases} \quad (17)$$

$$u(t) = \begin{cases} \frac{1}{a}\frac{A}{T}, & \frac{(t+\eta)}{T} \in [0,a), \\ -\frac{2}{b-a}\frac{A}{T}, & \frac{(t+\eta)}{T} \in [a,b], \\ \frac{1}{1-b}\frac{A}{T}, & \frac{(t+\eta)}{T} \in (b,1], \end{cases} \quad (18)$$

where T is the period of the oscillation, A the amplitude, $x_{0,(L,R)}$ the equilibrium position of the left or right moving wall and η a random number uniformly distributed in $[0,2\pi)$. Despite the randomization of the phase of oscillation, due to the breaking of the symmetry $u[m(T/2)+T/4-t]=-u[m(T/2)+T/4+t]$ $(m=0,1,2,\ldots)$, the acceleration rate in a FUM with one oscillating and one fixed wall and in a two-moving wall FUM is not identical. To clarify this, let us calculate the factor $R_{h,i}(n)$ $(i=L,R)$ in each setup, beginning from the FUM with one vibrating wall at $x=0$ and a fixed wall at $x=w$.

The change of the particle square velocity on the nth collision is given by the expression

$$\delta V_n^2 = V_n^2 - V_{n-1}^2 = -4V_n u_n + 4u_n^2, \quad (19)$$

where u_n is the wall velocity upon the nth collision and V_{n-1} is the particle velocity before this collision. The parameters a, b control the asymmetry of $x_L(t)$. In order to calculate the average over the phase $\langle\langle \delta V_n^2 \rangle\rangle$ within the framework of the SWA we need to separate the ensemble of particle trajectories in two sets. The first set consists of trajectories for which the acceleration process is identical to that of the exact model. The second set consists of trajectories for which the acceleration in the SWA is underestimated. Each zone is characterized by a fixed value of $\langle\langle \delta V_n^2 \rangle\rangle$. The zones in question can easily be determined graphically, given that the collision time predicted by the exact dynamics corresponds to the intersection of the particle trajectory and the piecewise linear curve representing the wall position as a function of time $x_L(t)$—see Fig. 4. The instant of collision as given by the SWA corresponds to the intersection of the particle trajectory and the t axis. This treatment requires the division of the interval $[0,T]$ in five zones—for the oscillation law of Eq. (17), as shown in Fig. 4. It is clear that, within some of the aforementioned zones the intersection of the particle trajectory with $x_L(t)$ and the t axis corresponds to instants characterized by different wall velocities, which, consequently, leads to different predictions for the energy gain of the particle by the SWA compared to the exact model. It is noted that the difference in the wall velocity due to the different predictions for the instant of collision between the two models is such that it always leads to an increased acceleration for the exact case, in accordance with the discussion of the previous section. Since the phase is uniformly distributed the size of the zones determines also the statistical weight of each zone. If we denote $\lambda=|V_n|T/A$ then the location and the size of the zones p_i are as follows:

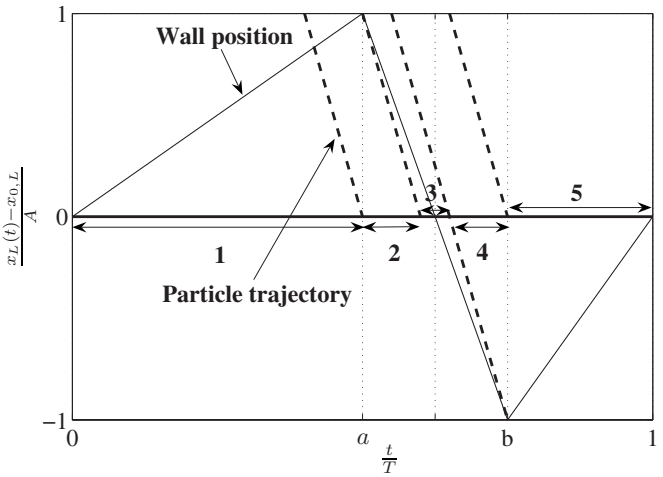

FIG. 4. The oscillation law for the FUM (with one oscillating wall). The borderlines of the zones discussed in the text are delimited by the dashed lines of slope $\lambda=|V_n|T/A$. The zones are also marked by double arrows.

$$\text{Zone 1: } \frac{t}{T} \in [0,a] \Rightarrow p_1 = a,$$

$$\text{Zone 2: } \frac{t}{T} \in \left[a, a+\frac{1}{\lambda}\right] \Rightarrow p_2 = \frac{1}{\lambda},$$

$$\text{Zone 3: } \frac{t}{T} \in \left[a+\frac{1}{\lambda}, b-\frac{1}{\lambda}\right] \Rightarrow p_3 = b-a-\frac{2}{\lambda},$$

$$\text{Zone 4: } \frac{t}{T} \in \left[b-\frac{1}{\lambda}, b\right] \Rightarrow p_4 = \frac{1}{\lambda},$$

$$\text{Zone 5: } \frac{t}{T} \in [b,1] \Rightarrow p_5 = 1-b.$$

Therefore, the average over the phase is given by

$$\langle\langle \delta V_n^2 \rangle\rangle = \sum_{i=1}^{5} p_i \delta V_{n,i}^2.$$

For the exact model using $u_0=A/T$ we obtain

$$\langle\langle \delta V_n^2 \rangle\rangle_{\text{exact}} = 4u_0^2\left[2\left(\frac{1}{a}+\frac{4}{b-a}+\frac{1}{1-b}\right) + \frac{1}{\lambda}\left(\frac{1}{a^2}-\frac{8}{(b-a)^2}+\frac{1}{(1-b)^2}\right)\right], \quad (20)$$

while using the SWA we get

$$\langle\langle \delta V_n^2 \rangle\rangle_{\mathrm{SWA}} = 4u_0^2\left(\frac{1}{a} + \frac{4}{b-a} + \frac{1}{1-b}\right). \tag{21}$$

Thus the function $R_h(n)$ is

$$R_{h,L}(n) = 2 + \frac{F(a,b)}{n}\sum_{i=1}^{n}\frac{1}{\lambda}, \tag{22}$$

with

$$F(a,b) = \frac{\dfrac{1}{a^2} - \dfrac{8}{(b-a)^2} + \dfrac{1}{(1-b)^2}}{\dfrac{1}{a} + \dfrac{4}{b-a} + \dfrac{1}{1-b}}.$$

Now we can perform also the averaging over the velocity distribution of the particles and obtain the final expression:

$$R_{h,L}(n) = 2 + \frac{u_0 F(a,b)}{n}\sum_{i=1}^{n}\left\langle\frac{1}{|V_{i-1}|}\right\rangle. \tag{23}$$

To derive a formula featuring explicitly the dependence on n it is necessary to determine $\langle 1/|V_{n-1}|\rangle$ as a function of n. Since the FUM under discussion is randomized, the acceleration of the particles can be described as a diffusion process in momentum space, i.e., by the Fokker-Planck equation. The solution of the Fokker-Planck equation (see Appendix A) assuming a perfectly reflective barrier at $|V|=0$ leads to the following asymptotic $(n \gg 1)$ expression for $\langle 1/V_{n-1}\rangle$:

$$\left\langle\frac{1}{|V_{n-1}|}\right\rangle \simeq \sqrt{\frac{\pi}{2}}\frac{1}{\sigma},$$

$$\sigma = \sqrt{g(a,b)(n-1) + \frac{V_0^2}{2}},$$

$$g(a,b) = 4u_0^2\left(\frac{1}{a} + \frac{4}{b-a} + \frac{1}{1-b}\right). \tag{24}$$

The summation after the substitution of Eqs. (24) into Eq. (23) yields

$$R_{h,L}(n) = 2 + \frac{u_0 F(a,b)}{n}\sqrt{\frac{\pi}{2g(a,b)}}\left[\zeta\left(\frac{1}{2},\frac{V_0^2}{2g(a,b)}\right) - \zeta\left(\frac{1}{2},n + \frac{V_0^2}{2g(a,b)}\right)\right], \tag{25}$$

where ζ stands for the generalized Riemann (Hurwitz) zeta function. For $n \gg 1$, $R_{h,L}(n) - 2 \propto 1/\sqrt{n} + O(1/n)$. Consequently, $R_{h,L}(n)$ for $n \to \infty$ approaches asymptotically the value 2 with a rate controlled by the parameters a, b. This is illustrated in Fig. 5, where numerical results for $R_{h,L}(n)$ obtained for $a=5\times10^{-3}$ and $b=0.67$ are shown along with the analytical result of Eq. (25). As demonstrated in this figure, for the particular choice of the parameter values, the function $R_{h,L}(n)$ deviates from the value 2 even for relatively large n.

Let us now discuss the case of a FUM consisting of one fixed wall at $x=0$ and one moving at $x=w$. As already mentioned, the two symmetrical FUM setups (moving wall on the right and fixed wall on the left and vice versa) do not lead to the same acceleration rate if the wall displacement on collision is taken into account, provided that the $u[m(T/2)+(T/4)-t]=-u[m(T/2)+(T/4)+t]$, $(m=0,1,2,\ldots)$ symmetry of the oscillation law is broken. This is so because, on the average, more energy is gained by a particle if it collides only with the right side of the wall than if it collides with its left side. Indeed, if we follow the steps outlined above then we obtain the following expression for $R_{h,R}(n)$ for a FUM with one moving wall on the right:

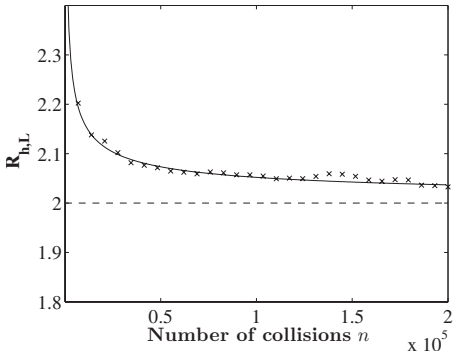

FIG. 5. Numerical results (×) as well as analytical results [see Eq. (25)]—solid line—for $R_{h,L}(n)$ in the original FUM, employing sawtooth driving for $u_0=0.01$, $a=5\times10^{-3}$, and $b=0.67$.

$$R_{h,R}(n) = 2 - \frac{u_0 F(a,b)}{n}\sqrt{\frac{\pi}{2g(a,b)}}\left[\zeta\left(\frac{1}{2},\frac{V_0^2}{2g(a,b)}\right) - \zeta\left(\frac{1}{2},n + \frac{V_0^2}{2g(a,b)}\right)\right], \tag{26}$$

which implies that a FUM with a moving wall on the right leads to a slower acceleration rate compared to its counterpart. Obviously, for the case of a two-moving wall FUM the factor R_h is given by

$$R_h(n) = \frac{R_{h,L}(n) + R_{h,R}(n)}{2} = 2. \tag{27}$$

Thus, for a two-moving wall FUM the correction factor for the increased acceleration due to the wall displacement on collision, considering that both walls follow the dynamics of Eq. (17), is independent of n and equal to that obtained for the case of harmonic driving [Eq. (16)]. In conclusion, $R_h(n)$ for the FUM setups with one moving wall depends on the number of collisions n and tends to the value $R_h(\infty)=2$, in a manner specified by the particular oscillation law, which is characterized here by the parameters a, b. On the other hand, when both walls of the FUM are allowed to move, then unless a specific choice for the dynamics of each of the walls is made, $R_h(n)$ is rendered independent of n and equals that obtained when a harmonic driving is considered.

E. Probability distribution function of the velocities

The focus of our attention now shifts to the probability distribution function (PDF) of the magnitude of the particle

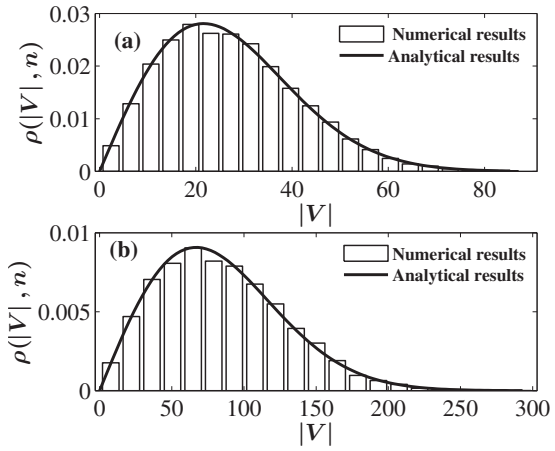

FIG. 6. Numerically computed PDF for the magnitude of the particle velocity using an ensemble of 10^4 trajectories and following the exact dynamics of Eq. (1) for (a) $n=5\times10^4$ and (b) $n=5\times10^5$ with $\epsilon=1/15$ and $V_0=100/15$. In each case, the analytical result given by Eq. (31) using the HWA is also shown (solid line).

velocity and number of collisions n, $\rho(|V|,n)$. We have shown that the evolution of $\langle V^2\rangle$ as a function of the number of collisions n can accurately be simulated by a random walk in momentum space $\langle V^2\rangle \propto n$, provided that the spatial motion of the walls is taken into account. Numerical as well as analytical treatments in setups similar to the present one suggest that $\rho(|V|,n)$ is described by a spreading Gaussian [31,32]. However, simulations of an ensemble of particles evolving in a two-wall phase randomized FUM assuming the driving to be harmonic and following the exact map of Eqs. (1a)–(1c) and (2) yield the histograms in Fig. 6, which illustrate the PDFs corresponding to snapshots for $n=5\times10^4$, 5×10^5 collisions. It is shown that, even if the initial PDF is a Gaussian, with increasing time, it is transformed to a Maxwell-Boltzmann-like distribution for a two-dimensional system, since the set of initial conditions leading to $|V|\ll1$ is vanishingly small for sufficiently long times.

The evolution of the PDF can be described as a diffusion process in momentum space. Therefore, the PDF can be obtained by solving the Fokker-Planck equation,

$$\frac{\partial}{\partial n}\rho(|V|,n) = -\frac{\partial}{\partial V}[B\rho(|V|,n)] + \frac{1}{2}\frac{\partial^2}{\partial V^2}[D\rho(|V|,n)], \tag{28}$$

where the transport coefficients B, D are

$$B(V) = \left(\frac{1}{\Delta n}\right)\int \Delta|V| P\, d(\Delta|V|), \tag{29a}$$

$$D(V) = \left(\frac{1}{\Delta n}\right)\int (\Delta|V|)^2 P\, d(\Delta|V|). \tag{29b}$$

In Eqs. (29a) and (29b) P is the probability of a particle possessing the velocity $|V|$ if it had the velocity $|V|-\Delta|V|$, Δn collisions earlier. Assuming that $\Delta n=1$, Eqs. (29a) and (29b) become $B(V)=\langle\delta|V|\rangle$ and $D(V)=\langle(\delta|V|)^2\rangle$, where $\langle\delta|V|\rangle$ is the mean increment of the magnitude of the particle velocity during one mapping period, i.e., in the course of one collision. From Eq. (1) it follows that $|V_{n+1}|=|V_n|\pm2u_n$, depending on the wall (left or right) with which a particle collides. Thus

$$\Delta|V| = \pm 2u_n. \tag{30}$$

In order to obtain $B(V)$, the average of Eq. (30) over the random phase component η_n must be calculated using the set of Eqs. (8a) and (8b), leading to $B(V)=2|I_1|$ where I_1 is given by Eq. (10). Therefore, $B(V)=\epsilon^2[\cos(1/V)/V]$. Due to the Fermi-acceleration mechanism, the majority of the particles of the ensemble for $n\gg1$, possesses velocities with a magnitude much larger than the corresponding initial value, i.e., $|V_n|\gg|V_0|>0$. Thus we can expand $B(V)$ to the leading order of $1/V$ to obtain $B(V)=\epsilon^2/V$. The diffusion coefficient $D(V)$ can be derived in a similar way. By raising Eq. (30) to the square we obtain, $D(V)=(\Delta|V|)^2=4u^2$. The integration over η_n leads to $D(V)=4I_2$, where I_2 is given by Eq. (11). Therefore, $D(V)=2\epsilon^2$.

Substituting the values of the transport coefficients into Eq. (28) and assuming a perfectly reflecting barrier at $|V|=0$ the following analytical expression for the PDF is obtained, which describes the magnitude of the particle velocity for $n\gg1$:

$$\rho(|V|,n) = \frac{1}{\sigma^2}|V|e^{-|V|^2/(2\sigma^2)}, \tag{31}$$

where $\sigma=\sqrt{(4\epsilon^2n+V_0^2)/2}$. In Figs. 6(a) and 6(b) it is clearly seen that this analytical result predicted by the HWA accurately reproduces the exact behavior of the system.

Furthermore, Fig. 7 shows the evolution of the mean value of the magnitude of the particle velocity $\langle|V|\rangle$ as a function of the number of collisions n obtained numerically for the exact dynamics. An analytical expression for $\langle|V|\rangle$ can easily be derived employing Eq. (31):

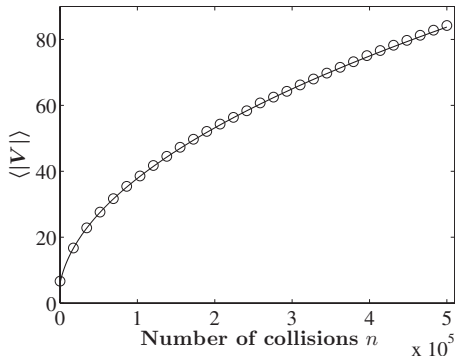

FIG. 7. Numerical results obtained by the iteration of the exact (○) map for the evolution of the ensemble mean magnitude of particle velocity $\langle|V|\rangle$ versus the number of collisions, n for $\epsilon=1/15$ and $|V_0|=100/15$. It is noted that $\langle|V|\rangle$ is measured in units of ωw. The analytical result according to the HWA, Eq. (32) (solid line), is also shown.

$$\langle |V| \rangle = \frac{\sqrt{\pi(4\epsilon^2 n + V_0^2)}}{2}. \tag{32}$$

For the sake of comparison this analytical result is also presented in Fig. 7. Once again, results yielded by the exact and the HWA map are in excellent agreement.

III. TIME-DEPENDENT LORENTZ GAS

In the theory of dynamical systems Lorentz gas [11] acts as a paradigm allowing us to address fundamental issues of statistical mechanics, for instance, ergodicity and mixing [33–35] and transport processes, such as diffusion in configuration space [36–41]. A generalization of the original periodic Lorentz gas model has recently been introduced [12] allowing the velocity of the scatterers to oscillate radially on a square lattice, i.e., *static* approximation. Due to the inherent strong chaotic dynamics of the static Lorentz gas, owing to the convex geometry of the scatterers, one intuitively expects [22] that the introduction of time dependence induces a Fermi mechanism of acceleration, resulting in unbounded growth of the velocity of the tracer particle. This is in contrast to the FUM, where, on the supposition of smooth periodic force functions, the particle energy remains bounded, due to the presence of a set of spanning KAM curves in the phase space [14,15] and only in the presence of external stochasticity does Fermi acceleration become feasible.

In the following, we study a time-dependent Lorentz gas consisting of harmonically oscillating scatterers on a triangular lattice. For this specific geometry, the horizon, i.e., the maximum distance traveled by an incident particle without suffering a collision, is finite [36], provided that the spacing w between neighboring disks is appropriately chosen. As mentioned above stochasticity is not needed in order to study Fermi acceleration. However, as will be shown, the presence or absence of stochasticity, as well as the specific manner in which it is introduced affects the acceleration process. The higher dimensionality of the system, in comparison to that of the FUM, provides us with another way to induce stochasticity without affecting the energy of the oscillating scatterers apart from phase randomization, namely by randomizing the direction of the oscillation axis. Therefore, stochasticity is induced by (a) performing a random phase shift to all scatterers when an incident particle exits the scattering area, through the addition of a random, uniformly distributed number $\eta \in [0, 2\pi)$ or by (b) rotating randomly the oscillation axis of all scatterers when again the particle exits the scattering area of the disk with which it collided; specifically, the inclination angle of the axis of oscillation of each disk is uniformly distributed in $[0, \pi)$. The imposed stochasticity simulates the effect of thermal fluctuations on the dynamics of the considered system. It is emphasized that the specific values of the random phase η or the axis inclination angles θ are updated once the particles escape the hexagonal elementary cell of the lattice. Within this approximation, memory effects are absent, and the simulation of thermal noise is easily implemented.

Although the *static* approximation has been successfully used in the past to understand the power-law increase of the mean velocity in a time-dependent Lorentz gas [12] it has also been shown that this approximation fails to describe correctly the increase of the mean particle velocity [27] in the case of a phase randomized harmonically driven periodic Lorentz gas, i.e., it systematically underestimates the numerically observed acceleration. However, motivated by the good agreement between the numerical results of the exact and the so called *hopping* map in Ref. [27] we utilize the latter in an effort to understand the dynamical correlations that lead to a higher acceleration in the harmonically driven Lorentz gas.

A. Exact map

The dynamics of a point particle suffering elastic collisions with a circular infinitely heavy harmonically driven scatterer are described by the following set of equations [42]:

$$0 = c_1(t_n - t_{n-1})^2 + c_2 \sin^2(\omega t_n + \eta_n) + c_3(t_n - t_{n-1}) + \sin(\omega t_n + \eta_n) + c_4(t_n - t_{n-1}) + c_5 \sin(\omega t_n + \eta_n) + c_6, \tag{33a}$$

$$\mathbf{r}_n = \mathbf{r}_{n-1} + \mathbf{V}_{n-1}(t_n - t_{n-1}), \tag{33b}$$

$$\mathbf{u}_{n,i} = \mathbf{A}_i \omega \cos(\omega t_n + \eta_n), \tag{33c}$$

$$\mathbf{V}_n = \mathbf{V}_{n-1} - 2[\hat{\mathbf{n}}(\mathbf{V}_{n-1} - \mathbf{u}_n)]\hat{\mathbf{n}}, \tag{33d}$$

where $\mathbf{A}_i$ is a vector directed along the randomly chosen axis of oscillation with magnitude equal to the amplitude of the oscillation of the ith scatterer, ω is the angular frequency of oscillation, η_n is a random number uniformly distributed in the interval $[0, 2\pi)$, t_n is the instant when the nth collision occurs, $\mathbf{r}_n$ the position vector of the particle at the instant t_n, $\mathbf{V}_n$ the particle velocity vector immediately after the collision, $\mathbf{u}_n$ the velocity of the scatterer, and finally $\hat{\mathbf{n}}$ the inward normal vector at the point of collision on the scatterer's boundary where collision occurs. Parameters $c_1, \ldots, c_6$ are given by

$$c_1 = \mathbf{V}_{n-1}^2,$$

$$c_2 = (\mathbf{A}_i)^2,$$

$$c_3 = -2\mathbf{V}_{n-1} \cdot \mathbf{A}_i,$$

$$c_4 = 2(\mathbf{r}_{n-1} - \mathbf{d}_{0,i}) \cdot \mathbf{V}_{n-1},$$

$$c_5 = 2(\mathbf{r}_{n-1} - \mathbf{d}_{0,i}) \cdot \mathbf{V}_{n-1},$$

$$c_6 = (\mathbf{r}_{n-1} - \mathbf{d}_{0,i})^2 - (R_i)^2,$$

where $\mathbf{d}_{0,i}$ is the position vector of the center of the ith scatterer at equilibrium and R_i its radius. For the sake of simplicity in the present analysis we assume that all the scatterers have the same amplitude of oscillation and radii. In order to eliminate the nonrelevant parameters, the dimensionless quantity $\epsilon = |\mathbf{A}|/w$ is introduced, where w denotes the spacing between the disk centers. Using as a length unit w and as

a time unit $1/\omega$ the map given by Eqs. (33a)–(33d) can be rewritten in a dimensionless form

$$0 = c_1(t_n - t_{n-1})^2 + c_2 \sin^2(t_n + \eta_n) + c_3(t_n - t_{n-1})\sin(t_n + \eta_n) + c_4(t_n - t_{n-1}) + c_5 \sin(t_n + \eta_n) + c_6, \tag{34a}$$

$$\mathbf{r}_n = \mathbf{r}_{n-1} + \mathbf{V}_{n-1}(t_n - t_{n-1}), \tag{34b}$$

$$\mathbf{u}_n = \epsilon[\cos(\theta)\hat{\imath} + \sin(\theta)\hat{\jmath}]\cos(t_n + \eta_n), \tag{34c}$$

$$\mathbf{V}_n = \mathbf{V}_{n-1} - 2[\hat{\mathbf{n}}(\mathbf{V}_{n-1} - \mathbf{u}_n)]\hat{\mathbf{n}}, \tag{34d}$$

where θ is the angle between the oscillation and the x-axis and $\hat{\imath}$, $\hat{\jmath}$ are the unitary vectors along the x and y axis, respectively. The parameters $c_1, \ldots, c_6$ become

$$c_1 = \mathbf{V}_{n-1}^2,$$

$$c_2 = \epsilon^2,$$

$$c_3 = -2\mathbf{V}_{n-1} \cdot \epsilon[\cos(\theta)\hat{\imath} + \sin(\theta)\hat{\jmath}],$$

$$c_4 = 2(\mathbf{r}_{n-1} - \mathbf{d}_{0,i}) \cdot \mathbf{V}_{n-1},$$

$$c_5 = 2(\mathbf{r}_{n-1} - \mathbf{d}_{0,i}) \cdot \mathbf{V}_{n-1},$$

$$c_6 = (\mathbf{r}_{n-1} - \mathbf{d}_{0,i})^2 - R^2.$$

B. Static approximation

As already mentioned above, the exact map describing the system dynamics is implicit with respect to the collision time, see Eq. (34a), rendering an analytical treatment of the acceleration process practically impossible. Moreover, the numerical solution of this implicit transcendental equation greatly complicates numerical simulations, making the long-term prediction of the particle acceleration a difficult task. In order to overcome these difficulties one usually resorts to the *static* approximation, according to which—as in the case of the FUM—the scatterer is considered to be fixed in configuration space, and yet when the particle suffers a collision with it the particle exchanges momentum as if the scatterer were oscillating. Thus the exact map is simplified to the following set of equations, which can now be solved explicitly for the collision time t_n:

$$0 = c_1(t_n - t_{n-1})^2 + c_2(t_n - t_{n-1}) + c_3, \tag{35a}$$

$$\mathbf{r}_n = \mathbf{r}_{n-1} + \mathbf{V}_{n-1}(t_n - t_{n-1}), \tag{35b}$$

$$\mathbf{u}_n = [\cos(\theta)\hat{\imath} + \sin(\theta)\hat{\jmath}]\epsilon\cos(t_n + \eta_n), \tag{35c}$$

$$\mathbf{V}_n = \mathbf{V}_{n-1} - 2[\hat{\mathbf{n}}(\mathbf{V}_{n-1} - \mathbf{u}_n)]\hat{\mathbf{n}}, \tag{35d}$$

where the parameters $c_1, \ldots, c_3$ are given by

$$c_1 = \mathbf{V}_{n-1}^2,$$

$$c_2 = 2(\mathbf{r}_{n-1} - \mathbf{d}_{0,i}) \cdot \mathbf{V}_{n-1},$$

$$c_3 = (\mathbf{r}_{n-1} - \mathbf{d}_{0,i})^2 - R^2. \tag{36}$$

It should be noted that if the combination of particle and disk velocity along the normal direction to the boundary at the point of collision is such that the normal particle velocity is not reversed after a collision, then it is done so factitiously, in order to prohibit the particle from traveling through the scatterer.

C. Hopping approximation

As explained in Sec. II B, instead of being treated as spatially static, scatterers within the *hopping* approximation are allowed to oscillate not only in velocity space but also in configuration space. Provided that the time of free flight between two successive collisions is small compared to the period of oscillation, i.e., high particle velocities, one can assume that a scatterer on the instant of the nth collision occupies the position it held on the $(n-1)$th collision, since the displacement of a disk between successive collisions is negligible. Thus, within the framework of this approximation, the deterministic component of the phase of the scatterer's position at the nth collision is taken to be equal to the deterministic phase component of the scatterer's velocity at the $(n-1)$th collision. This leads to an explicit mapping with regard to the instant of collision, t_n, which greatly speeds up numerical simulations, as the solution of transcendental equations is no longer necessary. At the same time this approach succeeds in describing statistical quantities of the system with great accuracy, as suggested by the numerical results presented in [27]. The dynamics of this approximation is described by the following set of equations:

$$\mathbf{d}_{n,i} = \mathbf{d}_{0,i} + [\cos(\theta)\hat{\imath} + \sin(\theta)\hat{\jmath}]\epsilon\sin(t_{n-1} + \eta_n), \tag{37a}$$

$$0 = c_1(t_n - t_{n-1})^2 + c_2(t_n - t_{n-1}) + c_3, \tag{37b}$$

$$\mathbf{r}_n = \mathbf{r}_{n-1} + \mathbf{V}_{n-1}(t_n - t_{n-1}), \tag{37c}$$

$$\mathbf{u}_n = [\cos(\theta)\hat{\imath} + \sin(\theta)\hat{\jmath}]\epsilon\cos(t_n + \eta_n), \tag{37d}$$

$$\mathbf{V}_n = \mathbf{V}_{n-1} - 2[\hat{\mathbf{n}}(\mathbf{V}_{n-1} - \mathbf{u}_n)]\hat{\mathbf{n}}, \tag{37e}$$

where $\mathbf{d}_{n,i}$ stands for the position vector of the ith scatterer's center on the nth collision.

D. Numerical results

It is convenient to express the dynamics of hard disk billiards in terms of canonical variables, which for the static Lorentz gas are the azimuthal angle $\phi \in [0, 2\pi)$ and the incidence angle $a \in [-\pi/2, \pi/2]$ between the inward normal vector to the surface $\hat{\mathbf{n}}$ and the particle velocity $\mathbf{V}$ before the collision. In the case of a billiard with oscillating scatterers, one has to introduce three more variables, namely the magnitude of the particle velocity $|\mathbf{V}|$, the angle between the axis of oscillation and the x axis $\theta \in [0, \pi)$ and the collision time

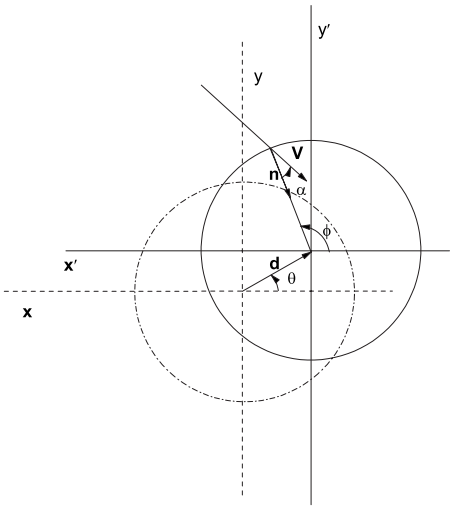

FIG. 8. The variables associated with an elementary collision process.

t. The different variables involved in the description of a collisional event are illustrated in Fig. 8.

Moreover, due to the fact that multiple collisions with the same disk are feasible, the incidence angle a no longer lies in the interval $[-\pi/2,\pi/2]$, but rather $a\in[-\pi,\pi]$. Given that only the normal component of the velocity changes in the process of scattering, and that the tangential component remains unchanged, the particle velocity vector after the collision is given by Eq. (34d). Assuming harmonic oscillation for the centers of the circular scatterers the boundary velocity at the moment of collision is $\mathbf{u}_n=\epsilon[\cos(\theta)\hat{\imath}+\sin(\theta)\hat{\jmath}]\cos(t_n+\eta_n)$. Therefore, the normal component of the boundary velocity vector at the time and point of collision is

$$u_{\perp,n}=\epsilon\cos(t_n+\eta_n)\cos(\pi-\phi_n+\theta_n). \tag{38}$$

Thus the square of the modulus of the particle velocity after the nth collision is

$$V_n^2=V_{n-1}^2-4u_{\perp,n}V_{n-1}\cos(a_n)+4(u_{\perp,n})^2. \tag{39}$$

Consequently, the change of the magnitude square of the particle velocity $\delta|V_n|^2=|V_n|^2-|V_{n-1}|^2$ is given by the equation

$$\delta|V|^2=-4u_{\perp,n}V_{n-1}\cos(a_n)+4(u_{\perp,n})^2. \tag{40}$$

In the static Lorentz gas, due to the mixing properties of the system, the probability distribution function (PDF) of a is given by [12]

$$\rho(a)=\frac{1}{2}\cos(a), \tag{41}$$

while the angle ϕ, follows a uniform distribution

$$\rho(\phi)=\frac{1}{2\pi}. \tag{42}$$

Generally, this does not apply for a billiard with time-dependent boundaries. In the present analysis we exclusively consider ensembles of trajectories with initial velocities

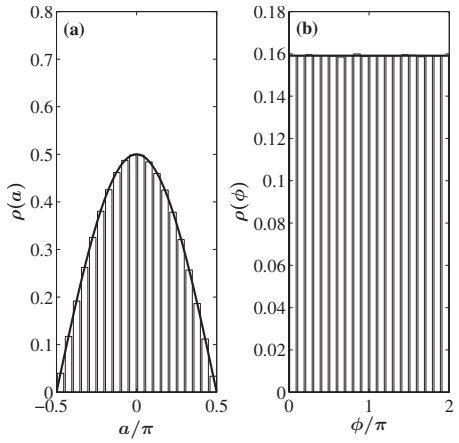

FIG. 9. Probability distribution functions (PDFs) of the (a) incidence angle a and (b) azimuthal angle ϕ. The theoretical predictions for the corresponding PDFs are also plotted (solid line).

larger than the maximum velocity of the scatterers, rendering multiple collisions with the same wall highly improbable and therefore negligible. It follows that the PDF of a can accurately be approximated by Eq. (41). These assumptions are validated numerically to a high accuracy, using an ensemble of 10^5 particle trajectories each one investigated for up to 10^4 collisions. Particles were randomly positioned close to the boundary of the scatterer, at a distance equal to $1.03R$ $-R$ denoting the radii of the scatterers—with a velocity vector, $\mathbf{V}=(|V|\cos z,|V|\sin z)$, of magnitude $|\mathbf{V}|=V=100/215$, with the angle z being a random variable uniformly distributed in the interval $[0,2\pi)$ and $\epsilon=1/215$. Results for the case of using phase randomization are shown in Fig. 9. It should be noted that all studied setups yield identical results for these distributions, regardless of the map type (exact or simplified), implemented in the numerical simulations.

In Figs. 10 and 11 the rms particle velocity V_{rms} is shown, as a function of the number of collisions n, for the case of

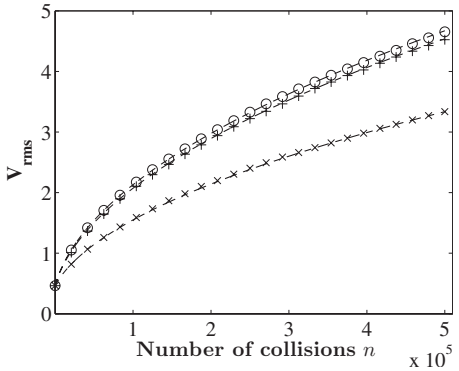

FIG. 10. Numerical results for the root mean square particle velocity V_{rms} as a function of the number of collisions n obtained by the iteration of the exact map, Eq. (34) (○) (with $\epsilon=1/215$ and $V_0=100/215$) for the driven Lorentz gas consisting of scatterers oscillating horizontally, with the oscillation phase shifted randomly when an incident particle leaves the elementary cell of the lattice. Corresponding results obtained utilizing the *hopping* (+) and *static* (×) approximative maps are also presented. The curves obtained by fitting with the model $\sqrt{\mu\epsilon^2n+V_0^2}$ are also plotted (dashed lines).

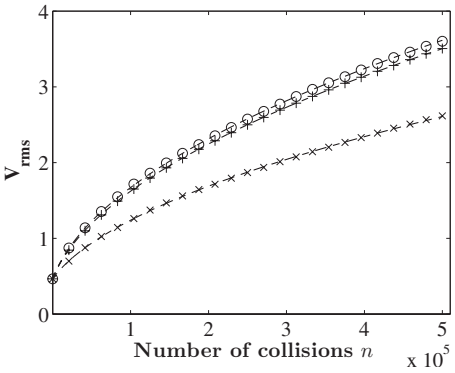

FIG. 11. Numerical results for the root mean square particle velocity, V_{rms}, as a function of the number of collisions n obtained by the iteration of the exact map (○) (with $\epsilon=1/215$ and $V_0=100/215$) for the setup with scatterers oscillating in a randomly chosen direction. Corresponding results obtained utilizing the *hopping* (+) and *static* (×) approximative maps are also presented. The curves acquired by fitting with the model $\sqrt{\mu\epsilon^2 n+V_0^2}$ are also plotted (dashed lines).

randomized oscillation phase and for the case where the scatterers are oscillating in a randomly chosen direction, i.e., $\theta \in [0,\pi)$. All the simulations are performed on the basis of an ensemble consisting of 10^4 particles, with an initial distribution for the magnitude of the particle velocities $\rho(|V|,0)=\delta(|V|-V_0)$, $V_0=100/215$, $\epsilon=1/215$, and $R=100/215$. These parameter values lead, in the static case, to a Lorentz gas with finite horizon and real space normal diffusion [36]. For the sake of comparison the same figures show the corresponding results obtained using the *static* as well as the *hopping* maps. Additionally, the curves obtained by fitting with the equation $\sqrt{\mu\epsilon^2 n+V_0^2}$, with μ being the fitting parameter, are also shown. The results of the fit are summarized in Table I.

In Figs. 10 and 11 it is evident that the *static* approximation fails to describe the evolution of the particle root mean square velocity. Specifically, a comparison between the values of μ in Table I, obtained by fitting the results yielded by the iteration of the exact and the *static* maps indicates that the asymptotic increase $(n \gg 1)$ of the square of particle velocity $\langle \delta V^2 \rangle$ is underestimated by a factor of two, both in the random phase as well as in the random oscillation axis setup. On the other hand, the *hopping* approximation, clearly provides a much more accurate description of the diffusion process (the small discrepancy between the results given by the exact and the *hopping* approximation is attributed to initial state effects, and becomes smaller the higher the initial velocity of the particles). Given that the fundamental difference between the *static* and the exact map is the motion of the disk in configuration space, the observed differences must be attributed to the disk displacement on collisions. The motion of the disk not only leads to additional fluctuations of the time of free flight as in the case of the stochastic FUM, but also affects the other variables that are intimately connected with the energy transfer between scatterer and projectile during a collision, namely the incident angle a and the azimuthal angle ϕ. The fluctuations caused by the scatterer displacement with respect to a and ϕ are again systematic, leading to an increased acceleration.

TABLE I. The values of the fitting parameter μ for the two system setups, i.e., with randomized direction of oscillation and randomized oscillation phase.

μ	Random axis	Random phase
Exact	$1.1880 \pm 2 \times 10^{-4}$	$1.997 \pm 4 \times 10^{-4}$
Hopping	$1.1151 \pm 3 \times 10^{-4}$	$1.8884 \pm 5 \times 10^{-4}$
Static	$0.6088 \pm 2 \times 10^{-4}$	$1.0009 \pm 7 \times 10^{-4}$

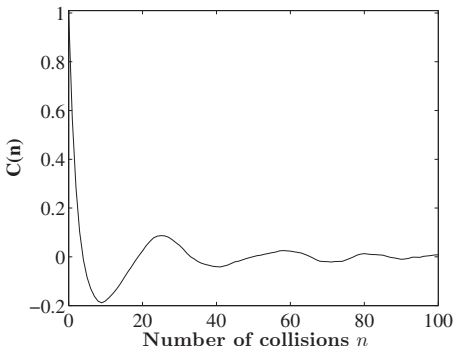

FIG. 12. Numerical results for the phase autocorrelation function $C(n)$ vs the number of collisions n for the Lorentz gas consisting of scatterers oscillating in a randomly chosen direction.

As already mentioned, the specific way the Lorentz gas is randomized affects the acceleration of the particles. Evidently, the numerical results obtained by the iteration of the exact map, Eq. (34), presented in Figs. 10 and 11 show that phase randomization leads to a more rapid acceleration compared to the acceleration observed in the setup with randomized direction of oscillation. The reduced acceleration in the case of randomizing the axis of oscillation is due to the autocorrelation of the phase. Indeed, as the particle velocity increases the time of free flight decreases, which correlates the oscillation phase of the nth collisions to the previous, $(n-1)$th, collision. This is demonstrated in Fig. 12, where numerical results of the autocorrelation function of the phase of oscillation $C(n)$ versus the number of collisions n are presented. It can be seen that the autocorrelation of the phase persists for more than 50 collisions.

E. Analytical results within the hopping approximation

In order to account for the dynamically induced correlations caused by the motion of the disks, a similar analysis to that conducted for the FUM should be performed using the corresponding *hopping* approximation, Eq. (37). For the sake of simplicity, we assume that the phase of oscillation upon collision is completely uncorrelated, even in a single time step, $(\Delta n)=1$. Consequently, our results apply only to the setup with randomized oscillation phase (and fixed oscillation axis). An analysis of the case of synchronized oscillations of the scatterers (with or without random direction of oscillation) will be carried out elsewhere [43].

Obviously, the disk displacement causes a shift of the values of the incident angle a, the azimuthal angle ϕ and the length of the free path l traveled by the incident particle on its collision course to a disk. This leads to a shift of the time of free flight $\delta t = l/|V|$. Therefore, assuming that the respective values of the variables on the nth collision, were the disk to be fixed on its equilibrium position, are a_n, ϕ_n, and l_n, Eqs. (38) and (40) can be rewritten as

$$\delta|V_n|^2 = -4u_{\perp,n}V_{n-1}\cos(a_n + \delta a_n) + 4u_{\perp,n}^2, \tag{43}$$

$$u_{\perp,n} = -\epsilon\cos\left(t_{n-1} + \frac{l_n + \delta l_n}{V_n} + \eta_n\right)\cos(\phi_n + \delta\phi_n), \tag{44}$$

where δa_n, $\delta\phi_n$, and δl_n denote the change to the values of the respective variables caused by the displacement of the scatterer on the nth collision. From geometrical considerations δa_n, $\delta\phi_n$, and δl_n can be expressed as a function of a_n, ϕ_n, l_n,

$$\delta l_n = R\left[\cos(\phi_n) - \cos(\phi_n + \delta\phi_n) - \frac{\epsilon}{R}\sin(t_{n-1} + \eta_n)\right] \times \sec(a_n + \phi_n), \tag{45}$$

$$\sin(a_n + \delta a_n) = \sin(a_n) - \frac{\epsilon}{R}\sin(t_{n-1} + \eta_n)\sin(a_n + \phi_n), \tag{46}$$

$$\delta\phi_n = -\delta a_n. \tag{47}$$

On the supposition of small oscillations the change δa_n, $\delta\phi_n$, δl_n caused by disk displacement to the angle variables and to the free particle path is small, i.e., δa_n, $\delta\phi_n$, $\delta l_n \ll 1$. Therefore, we can expand the left-hand side (LHS) of Eq. (46) to the leading order of δa_n to obtain an explicit equation for δa_n:

$$\delta a_n = -\frac{\epsilon}{R}\sec(a_n)\sin(t_{n-1} + \eta_n)\sin(a_n + \phi_n). \tag{48}$$

After the substitution of Eqs. (45), (47), and (48) to Eq. (43) and integration over η, ϕ, and a (for details see Appendix B), assuming that they follow the PDFs defined by Eqs. (41) and (42), we obtain a formula for the mean particle energy gain upon a collision, which reads

$$\delta V_n^2 = \epsilon^2\cos\left(\frac{\langle l\rangle}{V_n}\right) + \epsilon^2, \tag{49}$$

where $\langle l\rangle$ stands for the mean free path on the supposition of fixed scatterers at their corresponding equilibrium positions. In the limit of high particle velocities $\cos(\langle l\rangle/V_n)$ tends to unity. Thus the following asymptotic value of δV^2 is obtained:

$$\delta V_n^2 \simeq 2\epsilon^2. \tag{50}$$

It follows that the rms particle velocity is

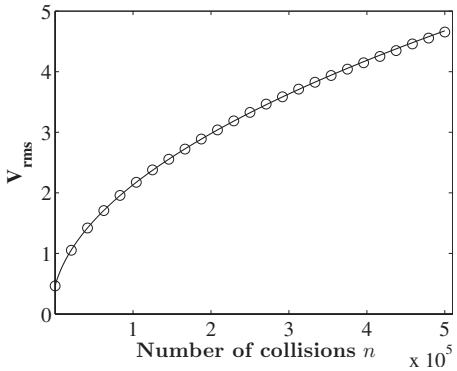

FIG. 13. Root mean square particle velocity, $V_{\rm rms}$, as a function of the number of collisions n obtained by the iteration of the exact map (○) (with $\epsilon = 1/215$ and $V_0 = 100/215$) for the case of scatterers with randomized phase of oscillation. For the sake of comparison, the analytical result of Eq. (51) is also shown (solid line).

$$\sqrt{\langle V_n^2\rangle} = \sqrt{\sum_{j=1}^{n}\langle\delta|V|_j^2\rangle + V_0^2} = \sqrt{2\epsilon^2 n + V_0^2}. \tag{51}$$

In Fig. 13 the analytical result given by Eq. (51) is shown together with numerical results obtained by the iteration of the exact map, Eq. (34), for the setup with randomized oscillation phase. Obviously, numerical and analytical results are in agreement, which proves that the small additional fluctuations both in the time of free flight and in the angle variables, a and ϕ due to the displacement of the scatterer, do not cancel out; on the contrary, they act systematically and account for the increased acceleration observed in the exact dynamics.

In order to obtain the value of the correction factor $R_h(n)$ for the Lorentz gas setup with randomized phase of oscillation, the mean increase of the square of particle velocity δV^2 must be also calculated within the framework of the *static* approximation. This can easily be done by averaging Eq. (40) over a, ϕ, and η to obtain $\delta V_n^2 = \epsilon^2$. Therefore,

$$R_h(n) = \frac{(\langle V^2\rangle - \langle V_0^2\rangle)_{\rm exact}}{(\langle V^2\rangle - \langle V_0^2\rangle)_{\rm SWA}} = \frac{\sum_{i=1}^{n}\langle\delta V_i^2\rangle_{\rm exact}}{\sum_{i=1}^{n}\langle\delta V_i^2\rangle_{\rm static}} \simeq 2. \tag{52}$$

It is worth noting that the value of $R_h(n)$, for the harmonically driven Lorentz gas with randomized phase of oscillation coincides with that obtained for the harmonically driven FUM (cf. Sec. II E).

Let us now direct our attention to the PDF of the magnitude of the particle velocity and number of collisions n, $\rho(|V|,n)$. The study of a square periodic Lorentz gas consisting of "breathing" circular scatterers, i.e., with oscillating boundary of the scatterer in the radial direction, in Ref. [12], conducted by means of the *static* approximation concluded that $\rho(|V|,n)$ is a sum of spreading Gaussians. Furthermore, general arguments presented in Ref. [31], where a random time-dependent Lorentz gas has been investigated, also suggest that $\rho(|V|,n)$ is a Gaussian. However, the numerical

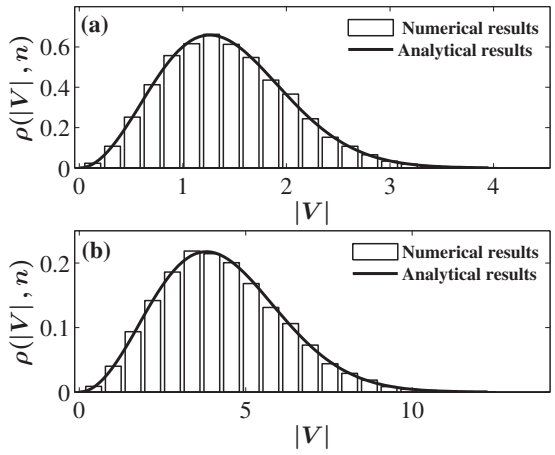

FIG. 14. Numerically computed PDF for the magnitude of the particle velocity using an ensemble of 10^4 trajectories and following the exact dynamics for: (a) $n=5\times10^4$ and (b) $n=5\times10^5$ with $\epsilon=1/215$ and $\|V_0\|=100/215$. In each case, the analytical result provided by Eq. (58) is also shown (solid line).

results presented in Fig. 14, which correspond to two snapshots for $n=5\times10^4$ and $n=5\times10^5$, obtained through the iteration of the exact map, point to the direction of $\rho(|V|,n)$ being a Maxwell-Boltzmann like distribution, corresponding to a *three-dimensional* system. Obviously, $\rho(|V|,n)$ can be analytically obtained through the solution of the Fokker-Planck equation (28). To do so the transport coefficients defined by Eqs. (29) and (30) must be calculated. Assuming that $\Delta n=1$ the transport coefficients coincide with the $\langle\delta|V_n|\rangle$and $\langle(\delta|V_n|)^2\rangle$. From Eq. (40) it follows that

$$|V_n| = |V_{n-1}|\sqrt{1-4\frac{u_{\perp,n}}{V_{n-1}}\cos(a_n+\delta a_n)+4\left(\frac{u_{\perp,n}}{V_{n-1}}\right)^2}. \tag{53}$$

Expanding Eq. (53) to the leading order of $u_{\perp,n}/V_n$ we get

$$\delta|V_n| = \frac{2(u_{\perp,n})^2\sin^2(a+\delta a_n)}{V_{n-1}} - 2u_{\perp,n}\cos(a). \tag{54}$$

Taking similar steps to those discussed in Appendix B we obtain

$$\langle\delta|V|\rangle = \frac{2\epsilon^2}{3V}, \tag{55}$$

$$\langle(\delta|V|)^2\rangle = \frac{2(V-2)\epsilon^2}{3V}. \tag{56}$$

Given that for $n\gg1$ the majority of the particles have velocities $V\gg1$, we can keep the dominant term in Eq. (56); thus

$$\langle(\delta|V_n|)^2\rangle \simeq \frac{2\epsilon^2}{3}. \tag{57}$$

The specific values of the coefficients together with reflective boundary conditions at $V=0$ lead to the following solution of the Fokker-Planck equation:

$$\rho(|V|,n) = \sqrt{\frac{2}{\pi}}\frac{1}{\sigma^3}|V|^2 e^{|V|^2/(2\sigma^2)},$$

$$\sigma = \sqrt{\frac{2\epsilon^2 n + V_0^2}{3}}. \tag{58}$$

In Fig. 14 the analytical result for the PDF, Eq. (58), is also plotted for the sake of comparison. Clearly, the analytics provides an accurate description for the PDF $\rho(|V|,n)$ for $n\gg1$. It must be noted, that the velocity distribution of the V_x, V_y components is symmetric, which implies that their is no drift velocity in the phase randomized driven Lorentz gas. This holds also for the case of the Lorentz gas with randomized direction of oscillation.

IV. SUMMARY AND CONCLUSIONS

The aim of this paper is twofold: First, to investigate the role of scatterer displacement upon collision in the Fermi acceleration mechanism developed in the well known FUM and a triangular periodic Lorentz gas, and second to obtain the corresponding time-evolving distributions of the particle velocities. In our analysis, we have assumed that either the phase or the axis of oscillation experiences a random shift after each collision with a particle, which mimics the effect of a noisy environment.

We have shown that the scatterer displacement produces a systematic effect in the acceleration process despite the imposed randomization. Specifically, the displacement of the scatterer leads to an increased acceleration compared to that observed when employing the standard static approximation. The increase in the acceleration observed in the FUM is related to small additional fluctuations of the time of free flight of the particles caused by the displacement of the disk. These fluctuations act *systematically* and lead to more energy gain or less energy loss in each collisional event. In the case of the driven Lorentz gas it was shown that a similar mechanism is at work, leading again to an increase in particle acceleration. Specifically, the displacement of the disks upon collision not only affects the time of the free flight of the particles, but it also alters the incident angle a and the azimuthal angle ϕ in such a way that leads again to more energy transfer from the disk to the particle and less energy loss.

The increase in acceleration was quantified by the function $R_h(n)$. We have shown that if the driving time law features the symmetry $u[m(T/2)+T/4-t]=-u[m(T/2)+T/4+t]$, $(m=0,1,2,\ldots)$ then $R_h(n)$ is almost independent of the number of collisions n, i.e., independent to the leading order of $\langle1/|V|\rangle\propto1/\sqrt{n}$, regardless of the specific billiard, being a FUM—with one or two moving walls—or a Lorentz gas. On the other hand, if the driving time law acting on the moving wall of the original FUM—with one fixed and one moving wall—is asymmetric then $R_h(n)$, again in the leading order of $\langle1/|V|\rangle$, is different from 2 for any finite number of collisions n and becomes equal to 2 only asymptotically. However, if the same force time law is considered in the context of a FUM with two, instead of one, moving walls then $R_h(n)$

is again independent of the number of collisions n and equals once more 2.

The investigation of the distribution functions of particle velocities in the FUM (with two moving walls or one moving and one fixed) revealed that irrespective of the specific driving of the billiard (sawtooth or harmonic) the same profile is obtained for $n \gg 1$, resembling a 2D Maxwell-Boltzmann distribution. This is in contrast to the result obtained by the application of the standard SWA, i.e., by not taking into account the displacement of the scatterer, where the corresponding PDFs are found spreading Gaussians. Moreover, we have shown that the application of the generalization of the *hopping* approximation leads to a similar profile for the PDF in the case of higher dimensional billiards, such as the phase randomized harmonically driven Lorentz gas, in which case it was shown that the PDF of the particle velocities is again Maxwell-Boltzmann-like (only in this case corresponding to a higher dimensional system). Another interesting aspect of this finding is that, though in the randomized FUM billiards and in the driven Lorentz gas no steady state of the distribution of the particle velocities exists, in all circumstances, i.e., independently of the specific billiard and driving, all the corresponding PDFs converge to a similar profile.

In all studied systems, we were able to obtain an analytical estimation of the evolution of the mean square velocity of the particles as a function of the number of collisions n, independently of the derivation of the distribution of particle velocities. For the setups considered herein it was found that in the presence of external randomization, $\sqrt{\langle V^2 \rangle} = V_{\mathrm{rms}} \propto \sqrt{n}$.

As a final remark, we note that the understanding of the dependence of particle acceleration behavior on the symmetries of the driving law, helps open up the prospect of designing specific devices combining driving laws with different symmetries in order to achieve a desired acceleration behavior.

ACKNOWLEDGMENT

The project is co-funded by the European Social Fund and National Resources (EPEAEK II) PYTHAGORAS.

APPENDIX A: SOLUTION OF THE FOKKER-PLANCK EQUATION FOR THE SAWTOOTH DRIVEN FUM

The evolution of the PDF in a randomized billiard, as discussed in Sec. II E, can be determined by the Fokker-Planck (FP) equation. Therefore, to determine $\langle 1/|V| \rangle$ as a function of the number of collisions, n, we must first obtain the PDF by solving the FP equation,

$$\frac{\partial}{\partial n}\rho(|V|,n) = -\frac{\partial}{\partial V}[B\rho(|V|,n)] + \frac{1}{2}\frac{\partial^2}{\partial V^2}[D\rho(|V|,n)], \tag{A1}$$

where the transport coefficients B, D are

$$B(V) = \left(\frac{1}{\Delta n}\right)\int \Delta|V| P\, d(\Delta|V|), \tag{A2a}$$

$$D(V) = \left(\frac{1}{\Delta n}\right)\int (\Delta|V|)^2 P\, d(\Delta|V|). \tag{A2b}$$

Assuming $\Delta n = 1$ the coefficients B, D coincide with the mean particle velocity increment $\delta|V|\rangle$ and the mean square of the particle velocity increment $\langle(\delta|V|)^2\rangle$, respectively, whereas, $\delta|V|$ is given by Eq. (30). Therefore, to determine the FP coefficients, the average of the wall velocity, $\langle\langle u_n \rangle\rangle$ and $\langle\langle u_n^2 \rangle\rangle$ over the oscillation phase must be calculated. Following the steps thoroughly discussed in Sec. II D, one finds

$$B = \langle \delta|V| \rangle = 2\frac{u_0^2}{|V|}\left(\frac{1}{a} + \frac{4}{b-a} + \frac{1}{1-b}\right), \tag{A3a}$$

$$D = \langle (\delta|V|)^2 \rangle = 4u_0^2\left[\left(\frac{1}{a} + \frac{4}{b-a} + \frac{1}{1-b}\right) + \frac{u_0}{|V|}\left(\frac{1}{a^2} - \frac{8}{(b-a)^2} + \frac{1}{(1-b)^2}\right)\right]. \tag{A3b}$$

Assuming the amplitude of wall velocity is small, $u_0 = \frac{A}{T} \ll 1$ and at the limit of high particle velocities $V \gg 1$ the first term on the RHS of Eq. (A3b) dominates and the coefficient $D(|V|)$ becomes asymptotically equal to

$$D \simeq 4u_0^2\left(\frac{1}{a} + \frac{4}{b-a} + \frac{1}{1-b}\right). \tag{A4}$$

Assuming reflective boundary conditions at $|V| = 0$ the solution of Eq. (A1) is

$$\rho(|V|,n) = \frac{|V|}{\sigma^2} e^{-|V|^2/(2\sigma^2)}, \tag{A5}$$

where

$$\sigma = \sqrt{4u_0^2\left(\frac{1}{a} + \frac{4}{b-a} + \frac{1}{1-b}\right)n + \frac{|V_0|^2}{2}}.$$

Thus, $\langle 1/|V_n| \rangle$ as a function of the number of collisions, n, reads

$$\left\langle \frac{1}{|V_n|} \right\rangle = \sqrt{\frac{\pi}{2}}\frac{1}{\sigma}. \tag{A6}$$

APPENDIX B

Assuming that the amplitude of oscillation A is small compared to the radii of the scatterers R the change caused by disk displacement to the angle variables δa_n, $\delta\phi_n$ and to the free particle path δl_n is small, i.e., δa_n, $\delta\phi_n$, $\delta l_n \ll 1$. Therefore, after the substitution of Eqs. (45) and (47) in Eq. (43), we expand the RHS of the resulting equation to the leading order of δa_n to obtain

$$\delta V_n^2 = \frac{8\cos^2(\phi_n)\cos\left(\frac{l_n}{V_{n-1}} + \eta_n + t_{n-1}\right)\sec(a_n+\phi_n)\sin(\eta_n + t_{n-1})\sin\left(\frac{l_n}{V_{n-1}} + \eta_n + t_{n-1}\right)\epsilon^3}{V_{n-1}}$$
$$+ 4\cos^2(\phi_n)\cos^2\left(\frac{l_n}{V_{n-1}} + \eta_n + t_{n-1}\right)\epsilon^2 + 4\cos(a_n)\cos(\phi_n)\sec(a_n+\phi_n)\sin(\eta_n + t_{n-1})\sin\left(\frac{l_n}{V_{n-1}} + \eta_n + t_{n-1}\right)\epsilon^2$$
$$+ 4V_{n-1}\cos(a_n)\cos(\phi_n)\cos\left(\frac{l_n}{V_{n-1}} + \eta_n + t_{n-1}\right)\epsilon$$
$$+ \delta a_n\left[\frac{16\cos(\phi_n)\cos\left(\frac{l_n}{V_{n-1}} + \eta_n + t_{n-1}\right)\sec(a_n+\phi_n)\sin(\phi_n)\sin(\eta_n + t_{n-1})}{V_{n-1}}\right.$$
$$\times \sin\left(\frac{l_n}{V_{n-1}} + \eta_n + t_{n-1}\right)\epsilon^3 + 8\cos(\phi_n)\cos^2\left(\frac{l_n}{V_{n-1}} + \eta_n + t_{n-1}\right)\sin(\phi_n)\epsilon^2$$
$$+ \frac{8R\cos^2(\phi_n)\cos\left(\frac{l_n}{V_{n-1}} + \eta_n + t_{n-1}\right)\sec(a_n+\phi_n)\sin(\phi_n)\sin\left(\frac{l_n}{V_{n-1}} + \eta_n + t_{n-1}\right)\epsilon^2}{V_{n-1}} - 4\cos(\phi_n)\sec(a_n+\phi_n)\sin(a_n)$$
$$\times\sin(\eta_n + t_{n-1})\sin\left(\frac{l_n}{V_{n-1}} + \eta_n + t_{n-1}\right)\epsilon^2 + 4\cos(a_n)\sec(a_n+\phi_n)\sin(\phi_n)\sin(\eta_n + t_{n-1})\sin\left(\frac{l_n}{V_{n-1}} + \eta_n + t_{n-1}\right)\epsilon^2$$
$$- 4V_{n-1}\cos(\phi_n)\cos\left(\frac{l_n}{V_{n-1}} + \eta_n + t_{n-1}\right)\sin(a_n)\epsilon + 4V_{n-1}\cos(a_n) \times \cos\left(\frac{l_n}{V_{n-1}} + \eta_n + t_{n-1}\right)\sin(\phi_n)\epsilon$$
$$\left. + 4R\cos(a_n)\cos(\phi_n)\sec(a_n+\phi_n)\sin(\phi_n)\sin\left(\frac{l_n}{V_{n-1}} + \eta_n + t_{n-1}\right)\epsilon\right]. \tag{B1}$$

The substitution of Eq. (48) into Eq. (B1) followed by integration over η_n yields

$$\langle\langle \delta V_n^2\rangle\rangle = 2\epsilon^2\cos^2(\phi_n)$$
$$+ 2\epsilon^2\cos\left(\frac{l_n}{V_{n-1}}\right)\cos(a_n)\cos(\phi_n)\sec(a_n+\phi_n)$$
$$+ \frac{2V_{n-1}\epsilon^2\sin\left(\frac{l_n}{V_{n-1}}\right)\sin(\phi_n)\sin(a_n+\phi_n)}{R}$$
$$- \frac{2V_{n-1}\epsilon^2\cos(\phi_n)\sin\left(\frac{l_n}{V_{n-1}}\right)\sin(a_n+\phi_n)\tan(a_n)}{R}$$
$$- \epsilon^2\cos\left(\frac{l_n}{V_{n-1}}\right)\sin(2\phi_n)\tan(a_n+\phi_n). \tag{B2}$$

The length of the free path l_n traveled by a particle between any two successive collisions, assuming the disk with which it experiences its nth collision to be fixed at its equilibrium position, is itself a function of the angle variables a_n and ϕ_n as well as the respective ones upon the previous collision, a_{n-1} and ϕ_{n-1}. Moreover, l_n also depends on the phase of oscillation at its previous, $(n-1)$th, collision due to the displacement of the disk at the previous step. However, as explained in Sec. II C it is the displacement of the scatterer at its nth collision that affects the energy transfer on the same collision. In other words, the variation of l_n does not systematically affect the energy gain of a particle during a collision. Therefore, to facilitate analytical treatment in Eq. (B2) we substitute l_n with its mean value $\langle l\rangle$. The final step is to obtain the mean value of δV_n^2 with respect to a_n and $\phi_n$using the PDFs given by Eqs. (41) and (42). The integration yields

$$\delta\langle V_n^2\rangle = \epsilon^2\left[\cos\left(\frac{\langle l\rangle}{V_{n-1}}\right) + 1\right]. \tag{B3}$$

[1] E. Fermi, Phys. Rev. **75**, 1169 (1949).
[2] R. Blandford and D. Eichler, Phys. Rep. **154**, 1 (1987).
[3] A. Veltri and V. Carbone, Phys. Rev. Lett. **92**, 143901 (2004).
[4] K. Kobayakawa, Y. S. Honda, and T. Samura, Phys. Rev. D **66**, 083004 (2002).
[5] M. A. Malkov, Phys. Rev. E **58**, 4911 (1998).
[6] G. Michalek, M. Ostrowski, and R. Schlickeiser, Sol. Phys. **184**, 339 (1999).
[7] A. V. Milovanov and L. M. Zelenyi, Phys. Rev. E **64**, 052101 (2001).
[8] F. Saif, I. Bialynicki-Birula, M. Fortunato, and W. P. Schleich, Phys. Rev. A **58**, 4779 (1998).
[9] A. Steane, P. Szriftgiser, P. Desbiolles, and J. Dalibard, Phys. Rev. Lett. **74**, 4972 (1995).
[10] G. Lanzano *et al.*, Phys. Rev. Lett. **83**, 4518 (1999).
[11] H. A. Lorentz, Proc. R. Acad. Sci. Amsterdam **7**, 438 (1905).
[12] A. Yu. Loskutov, A. B. Ryabov, and L. G. Akinshin, JETP **89**, 966 (1999); J. Phys. A **33**, 7973 (2000).
[13] S. Ulam, in *Proceedings of the Fourth Berkley Symposium on Mathematics, Statistics, and Probability* (California University Press, Berkeley, 1961), Vol. 3, p. 315.
[14] M. A. Lieberman and A. J. Lichtenberg, Phys. Rev. A **5**, 1852 (1972).
[15] A. J. Lichtenberg and M. A. Lieberman, *Regular and Chaotic Dynamics*, Applied Mathematical Sciences, Vol. 38 (Springer-Verlag, NewYork, 1992).
[16] P. J. Holmes, J. Sound Vib. **84**, 173 (1982).
[17] R. M. Everson, Physica D **19**, 355 (1986).
[18] Z. J. Kowalik, M. Franaszek, and P. Pieranski, Phys. Rev. A **37**, 4016 (1988).
[19] S. Warr *et al.*, Physica A **231**, 551 (1996).
[20] S. Celaschi and R. L. Zimmerman, Phys. Lett. A **120**, 447 (1987).
[21] E. D. Leonel, J. K. da Silva, and S. O. Kamphorst, Physica A **331**, 435 (2004).
[22] E. D. Leonel and P. V. E. McClintock, J. Phys. A **38**, 823 (2005).
[23] A. J. Lichtenberg, M. A. Lieberman, and R. H. Cohen, Physica D **1**, 291 (1980).
[24] E. D. Leonel, P. V. E. McClintock, and J. K. da Silva, Phys. Rev. Lett. **93**, 014101 (2004).
[25] E. D. Leonel and P. V. E. McClintock, Phys. Rev. E **73**, 066223 (2006).
[26] D. G. Ladeira and J. K. da Silva, Phys. Rev. E **73**, 026201 (2006).
[27] A. K. Karlis, P. K. Papachristou, F. K. Diakonos, V. Constantoudis, and P. Schmelcher, Phys. Rev. Lett. **97**, 194102 (2006).
[28] G. M. Zaslavskii and B. V. Chirikov, Sov. Phys. Dokl. **9**, 989 (1965).
[29] A. Brahic, Astron. Astrophys. **12**, 98 (1971).
[30] W. H. Press, S. A. Teukolsky, W. T. Vetterling, and B. P. Flannery, *Numerical Recipes in Fortran 77: The Art of Scientific Computing*, 2nd ed. (Cambridge University Press, Cambridge, England, 1992), pp. 352–355.
[31] F. Bouchet, F. Cecconi, and A. Vulpiani, Phys. Rev. Lett. **92**, 040601 (2004).
[32] E. Ott, *Chaos in Dynamical Systems* (Cambridge University Press, Cambridge, UK, 1993).
[33] Ya. G. Sinai, Russ. Math. Surveys **27**, 21 (1972); **25**, 137 (1970).
[34] L. A. Bunimovich, Commun. Math. Phys. **65**, 295 (1979).
[35] L. A. Bunimovich and Ya. G. Sinai, Commun. Math. Phys. **78**, 247 (1980); **78**, 479 (1980).
[36] J. Machta and R. Zwanzig, Phys. Rev. Lett. **50**, 1959 (1983).
[37] H. v. Beijeren, Rev. Mod. Phys. **54**, 195 (1982).
[38] P. Gaspard, *Chaos, Scattering, and Statistical Mechanics* (Cambridge University Press, Cambridge, UK, 1998).
[39] R. Klages and C. Dellago, J. Stat. Phys. **101**, 145 (2000).
[40] C. P. Dettmann, in *Encyclopaedia of Mathematical Sciences*, edited by D. Szasz (Springer, Berlin, 2000), Vol. 101, p. 315.
[41] D. N. Armstead, B. R. Hunt, and E. Ott, Phys. Rev. E **67**, 021110 (2003).
[42] P. K. Papachristou, F. K. Diakonos, E. Mavrommatis, and V. Constantoudis, Phys. Rev. E **64**, 016205 (2001).
[43] A. K. Karlis *et al.* (unpublished).